Plasma Sources Sci. Technol. **17** (2008) 035024 (11pp) doi:10.1088/0963-0252/17/3/035024

Repetitively pulsed atmospheric pressure discharge treatment of rough polymer surfaces: I. Humid air discharges

Ananth N Bhoj[1,3] **and Mark J Kushner**[2,4]

[1] Department of Chemical and Biomolecular Engineering, University of Illinois, Urbana, IL 61801, USA
[2] Department of Electrical and Computer Engineering, Iowa State University, Ames, IA 50011, USA

E-mail: ananth.bhoj@novellus.com and mjk@iastate.edu

Received 8 March 2008, in final form 29 May 2008
Published 31 July 2008
Online at stacks.iop.org/PSST/17/035024

Abstract
Plasmas generated at atmospheric pressure are used to functionalize the surfaces of polymers by creating new surface-resident chemical groups. The polymers used in textiles and biomedical applications often have non-planar surfaces whose functionalization requires penetration of plasma generated species into sometimes complex surface features. In this regard, the atmospheric pressure plasma treatment of a rough polypropylene surface was computationally investigated using a two-dimensional plasma hydrodynamics model integrated with a surface kinetics model. Repetitively pulsed discharges produced in a dielectric barrier–corona configuration in humid air were considered to affix O. Macroscopic non-uniformities in treatment result from the spatial variations in radical densities which depend on the polarity of the discharge. Microscopic non-uniformities arise due to the higher reactivity of plasma produced species, such as OH radicals, which are consumed before they can diffuse deeper into surface features. The consequences of applied voltage magnitude and polarity, and the relative humidity on discharge dynamics and radical generation leading to surface functionalization, are discussed.

1. Introduction

Plasma functionalization of polymers entails the modification of the topmost surface layers with chemically different atoms or functional groups to modify surface properties. For example, atmospheric pressure plasmas in air [1–3] are commonly used to functionalize the surfaces of hydrocarbon polymeric materials by affixing O-containing groups. Given the hydrocarbon backbone (represented by RH) some of these groups are alcohols (R–OH), peroxy (R–OO•), carbonyl (R–C=O) and acid (O=R–OH) [4, 5]. Higher O/C ratios in the chemical composition of the topmost layers increase the surface energy and so improve properties such as adhesion, wettability or reactivity.

There is interest in using plasmas to modify the surface properties of natural and synthetic textiles as being more environmentally friendly than wet processing [6, 7]. Plasma treatment of textile fibers improves shrink resistance, hydrophilicity and color fastness [8, 9]. Textile fabrics usually consist of fibers in a warp and weft arrangement, creating surface features of a few to tens of micrometers [10]. Since the entire fabric surface is not completely exposed to the discharge, the ability of plasma produced reactive species to penetrate into surface features is important to the quality and uniformity of treatment [11–13].

Biomedical surfaces are also often non-planar and rough, and functionalized by plasmas to enhance (or prevent) desired interactions with living cells [14]. For example, plasma treated implants and grafts have been used for many years. Polymer substrates are also modified using plasmas for cell micro-patterning where selectively activated regions of the surface are affixed with functional groups which promote cell adhesion [15]. Tissue engineering routinely involves the functionalization of topologically rough scaffold-like surfaces to promote cell adhesion and proliferation [16, 17].

[3] Present address: Novellus Systems, Inc., 3011 N. 1st St, San Jose, CA 95134, USA.
[4] Author to whom any correspondence should be addressed.

Common to both of these classes of applications is the desire that the plasma process uniformly treats the surface independently of the local topography which requires that reactive plasma produced species penetrate into this roughness. Gaining a deeper understanding of the interaction between gas phase transport processes and surface reaction pathways leading to functionalization will enable optimization of the relative abundance of functional groups on the surface and even the creation of tailored functional group gradients [18].

In this paper, and in part II [19], we discuss the results from a multiscale computational investigation of the plasma treatment of rough and porous polypropylene (PP) surfaces in a repetitively pulsed atmospheric pressure corona discharge using an integrated two-dimensional plasma hydrodynamics–surface kinetics model. Discharges in air can efficiently functionalize PP surfaces with O-containing groups due to the abundant generation of reactive oxygen containing gas phase species such as O, OH and O_3, and the fact that O_2 can affix to radical sites. Although charged particles do not play a large role in directly functionalizing surfaces, we found that the charged particle dynamics indirectly influence the uniformity and the magnitude of treatment. For example, the polarity of the voltage pulse has an effect on the extent of plasma penetration into rough features. With positive corona discharges, the electron density near small features (a few to many micrometers) is low due to the formation of a cathode fall-like region, thereby reducing the amount of electron impact dissociation in the immediate vicinity of the feature. Radicals take longer to penetrate into features by diffusion whereas recombination of positive ions increases the supply radicals at the surface.

We found that variations in the relative humidity affect the microscopic uniformity of surface functionalization. In low humidity discharges, gas phase OH radicals are generated close to the surface as products of H abstraction by O atoms, in densities comparable to that produced by electron impact of H_2O in higher humidity discharges. At higher applied voltages, the energy deposition per pulse increases, producing more O atoms. This results in a higher overall degree of functionalization but at the cost of increased macroscopic non-uniformity.

The model used in the investigation is described in section 2 and the results from these simulations are discussed in section 3. Our concluding remarks are in section 4.

2. Description of the model and reaction mechanisms

The two-dimensional modeling platform, *non-PDPSIM*, has closely coupled modules addressing plasma dynamics and gas phase kinetics. These modules are the same as described in [20]. Briefly, the plasma dynamics module is used to solve Poisson's equation for the electric potential simultaneously with the multi-fluid charged and neutral species conservation equations on an unstructured mesh. Poisson's equation and the conservation equations for charged species are simultaneously solved. The conservation equations for electron temperature, neutral species densities and flow properties are sequentially integrated in a time-splicing manner following the updates of Poisson's equation and charged particle densities. These updates are then followed by integration of the continuity equations for surface-resident species. A radiation transport module is used to track photons emitted from designated excited species. These photons photoionize the gas and interact with the polymer surface.

The model is capable of simulating the repetitively pulsed discharges (a few to tens of kilohertz). In these discharges, the duration of the pulse is typically short (10s ns at most) compared with the time between pulsing (usually $\geqslant$100s μs). During the discharge pulse, all of the equations addressing electrostatics, and charged and neutral particle transport are solved. After the termination of the pulse and charged particle densities have diminished to negligible values, the interpulse period (IP) begins. During the IP, only the conservation equations for neutral transport, and gas and surface reaction kinetics are integrated. After the IP, the discharge is reinitiated. This procedure is continued until quasi-steady state conditions are achieved. At this point, and with prior knowledge that further evolution of the surface coverages will not significantly affect the plasma properties, the time-varying fluxes of all plasma species at all locations on the surfaces are recorded during an additional discharge pulse and IP. The recorded fluxes are then interpolated as a function of time while executing the surface kinetics module (SKM) for additional pulses and IPs.

The SKM is the same as that described in [20]. The SKM consists of a modified surface site-balance algorithm implemented at the nodes of specified materials that border the plasma. Briefly, the initial conditions for the SKM are the surface coverages of species found on the virgin polymer. The SKM accepts fluxes of gas phase species and photons, and implements a user-specified surface reaction mechanism consisting primarily of gas phase species reacting on the surface sites. The mechanism also allows for photochemistry and reactions between surface sites. Outputs from the SKM include the fractional coverage of surface-resident species and returning fractions for gas phase reactants and products.

The reaction mechanism used for humid air gas phase chemistry is essentially the same as that described in [21]. Gas species include N_2, $N_2(A\,^3\Sigma)$, N_2^{**}, N_2^+, N^+, N_4^+, N, N(^{2}D), O_2, $O_2(a\,^1\Delta)$, $O_2(b\,^1\Sigma)$, O_2^+, O_2^-, O^-, O(^{1}D), O(^{1}S), O^+, O, O_3, H_2O, H_2O^+, H_2, H, OH and HO_2. N_2^{**} nominally denotes $N_2(b\,^1\Pi,\ b'\ ^1\Sigma)$ but is used as a lumped state including transitions higher than $N_2(A\,^3\Sigma)$. In order to propagate the positive corona streamer, photoionization was included with N_2^{**} being the emitting species with a lifetime of 5 ns, producing photoionization of O_2 with a cross section of 10^{-19} cm^{-2}. Electron impact reactions with N_2, O_2 and H_2O including vibrational excitation, electronic excitation, attachment and ionization are included in the calculation of the electron energy distribution for generating rate coefficients even though the vibrational states are not explicitly included in the model.

The most important gas phase reactions of relevance to surface treatment consist of neutral chemistry, initiated by

electron impact reactions of O_2 and H_2O producing O and OH radicals,

$$e + O_2 \rightarrow O + O + e, \quad (1)$$

$$e + H_2O \rightarrow H + OH + e. \quad (2)$$

At atmospheric pressure, three-body reactions dominate the radical kinetics, where O reacts with O_2 to form O_3 and H reacts with O_2 to form HO_2,

$$O + O_2 + M \rightarrow O_3 + M \quad (k = 6.9 \times 10^{-34} T_g^{-1.25}\ \mathrm{cm^6\ s^{-1}}), \quad (3)$$

$$H + O_2 + M \rightarrow HO_2 + M \quad (k = 6.1 \times 10^{-32} T_g^{-1.6}\ \mathrm{cm^6\ s^{-1}}), \quad (4)$$

where k is the rate coefficient at room temperature unless there is specific temperature dependence noted. There are few major gas phase consumption pathways for O_3 at room temperature and so it tends to accumulate from pulse to pulse. O_3 does react at slow rates with H to form OH, with O to form O_2 and with OH to form HO_2,

$$H + O_3 \rightarrow OH + O_2 \quad (k = 1.4 \times 10^{-10} e^{-470/T_g}\ \mathrm{cm^3\ s^{-1}}), \quad (5)$$

$$O + O_3 \rightarrow O_2 + O_2 \quad (k = 8 \times 10^{-12} e^{-2060/T_g}\ \mathrm{cm^3\ s^{-1}}), \quad (6)$$

$$OH + O_3 \rightarrow HO_2 + O_2 \quad (k = 1.9 \times 10^{-12} e^{-1000/T_g}\ \mathrm{cm^3\ s^{-1}}). \quad (7)$$

O_3 does undergo other dissociative processes, for example, reacting with O_2 to form O_2 and O. This process, as well as others, are included in the reaction mechanism however they are important only at higher gas temperatures than of interest here.

HO_2 reacts slowly with O, H and OH forming radicals or stable products. OH and O react mutually at slow rates to form H,

$$HO_2 + O \rightarrow OH + O_2 \quad (k = 2.9 \times 10^{-11} e^{-200/T_g}\ \mathrm{cm^3\ s^{-1}}), \quad (8)$$

$$HO_2 + OH \rightarrow H_2O + O_2 \quad (k = 8 \times 10^{-11}\ \mathrm{cm^3\ s^{-1}}), \quad (9)$$

$$HO_2 + H \rightarrow H_2O + O \quad (k = 2.4 \times 10^{-12}\ \mathrm{cm^3\ s^{-1}}), \quad (10)$$

$$O + OH \rightarrow H + O_2 \quad (k = 2.3 \times 10^{-11} e^{110/T_g}\ \mathrm{cm^3\ s^{-1}}). \quad (11)$$

The surface reaction mechanism is essentially the same as that discussed in [20]. Surface reactions are initiated by H abstraction from the hydrocarbon backbone (RH) by gas phase radicals, principally O and OH, creating active surface alkyl sites (R•). The probability of a reaction may vary with the local H bonding at the site of the C atom due to bond polarity effects, and that variation is accounted for in the mechanism. As a result, secondary and primary C atom sites were less reactive than tertiary and secondary sites by a factor of 5–10, respectively. The initiating steps are

$$RH + O \rightarrow R^\bullet + OH \qquad p = 10^{-3}, \quad (12)$$

$$RH + OH \rightarrow R^\bullet + H_2O \qquad p = 0.1, \quad (13)$$

where p is the probability of reaction for the tertiary sites. R• sites rapidly react with O and O_3 to form alkoxy (R–O•) groups,

$$R^\bullet + O \rightarrow R\text{–}O^\bullet \qquad p = 0.1, \quad (14)$$

$$R^\bullet + O_3 \rightarrow R\text{–}O^\bullet + O_2 \qquad p = 1.0. \quad (15)$$

In contrast, the reaction of R• sites with O_2 to form peroxy (R–OO•) groups has a lower probability, but due to the larger densities of O_2 are fairly rapid,

$$R^\bullet + O_2 \rightarrow R\text{–}OO^\bullet \qquad p = 10^{-3}. \quad (16)$$

Reactions between surface sites also occur (with the rate coefficients specified in units of $\mathrm{cm^2\ s^{-1}}$). For example, abstraction of H atoms from surrounding sites by R–O• groups results in alcohol (R–OH) groups with a rate coefficient of 10^{-16}–$10^{-15}\ \mathrm{cm^2\ s^{-1}}$,

$$R\text{–}O^\bullet + RH \rightarrow R\text{–}OH + R^\bullet, \quad (17)$$

which leaves an alkyl radical to sustain further reactions. Alternatively the C–C bond at the R–O• site cleaves, leading to chain scission and the formation of carbonyl (HR=O) groups, and the creation of a new R• radical site at rates of $10^3\ \mathrm{s^{-1}}$,

$$R\text{–}O^\bullet \rightarrow R{=}O + R^\bullet. \quad (18)$$

The reaction of carbonyl groups with O and OH creates carbonyl radicals (•R=O), which, upon further reaction with OH, results in an acid group (HO–R=O),

$$HR{=}O + O \rightarrow {}^\bullet R{=}O + OH, \quad (19)$$

$$HR{=}O + OH \rightarrow {}^\bullet R{=}O + H_2O, \quad (20)$$

$${}^\bullet R{=}O + OH \rightarrow HO - R{=}O. \quad (21)$$

Continued chain scission similar to that occurring with alkoxy groups leads to the formation of CO_2, a terminal step in the reaction chain,

$${}^\bullet R = O + O \rightarrow RH + CO_2. \quad (22)$$

Other termination steps include the recombination of alkyl radicals on the backbone with H and OH radicals,

$$R^\bullet + H \rightarrow RH \qquad p = 0.2, \quad (23)$$

$$R^\bullet + OH \rightarrow R\text{–}OH \qquad p = 0.2. \quad (24)$$

The contribution of ions to the surface reactions in atmospheric pressure discharges is less clear. The high collisionality of atmospheric pressure discharges results in ions having near thermal energy close to the surface. It is feasible for ions arriving at the surface to contribute to surface chemical reactions in a manner similar to their neutral radical counterparts. For instance, thermal O^+ and O_2^+ can react on the surface in a manner similar to O and O_2 since they are typically neutralized prior to striking the surface. Non-reactive ions may still break chemical bonds due to the potential energy they bring or due to secondary electron emission. There are no specific data available in the literature for

the secondary electron emission coefficient (γ) on dielectric surfaces due to ion bombardment at atmospheric pressure though estimates give $\gamma = 0.01$ [22]. In the context of surface chemical reactions, ion bombardment accompanied by secondary electron emission most likely leads to the formation of alkyl sites (R•). A sensitivity analysis was performed by varying γ from 10^{-3}–1.0. It was determined that for the transient discharges investigated in this work, the contributions of ion-initiated reactions to surface functionalization are not significant due to the short pulse durations.

Photons emitted from the plasma are thought to play a more important role in surface kinetics [23–25]. UV photons emitted with energies greater than 4–5 eV can cleave C–C bonds forming alkyl sites. Skurat, *et al* [26] proposed that UV photochemistry on hydrocarbon polymers proceeds via three major pathways, the dominant one being the elimination of H_2 forming adjacent alkyl radical sites (–·RR·–). These sites have a higher probability of undergoing scission to form R• sites than recombining [23],

$$RH + h\nu \rightarrow {}^{\bullet}RR^{\bullet} + H_2, \tag{25}$$

$${}^{\bullet}RR^{\bullet} \rightarrow R{=}R, \tag{26}$$

$${}^{\bullet}RR^{\bullet} \rightarrow R^{\bullet} + R^{\bullet}. \tag{27}$$

The other two pathways result in the formation of R• radicals by breaking either the C–H bond releasing atomic hydrogen or the C–C bond scission in the PP backbone,

$$RH + h\nu \rightarrow R^{\bullet} + H, \tag{28}$$

$$RH + h\nu \rightarrow R^{\bullet} + R^{\bullet}. \tag{29}$$

Skurat *et al* [26] estimated the relative rates of equation (29) are about 4–5 times faster than those of equation (28). In this work, the total quantum yield of photons leading to the formation of alkyl (R•) sites was taken to be 0.2 [27].

Surface radicals (R•) on adjacent backbones can react with each other to crosslink [28–31]. The crosslinking reactions included in the mechanism include

$$R^{\bullet} + R^{\bullet} \rightarrow R \times R \qquad p = 10^{-15}\,\mathrm{cm^2\,s^{-1}}, \tag{30}$$

$$2({}^{\bullet}RR^{\bullet}) \rightarrow R \times R \qquad p = 10^{-15}\,\mathrm{cm^2\,s^{-1}}, \tag{31}$$

where × indicates a crosslinked site.

3. Functionalization of rough surfaces in humid air discharges

The humid air, atmospheric pressure discharge functionalization of PP with rough surface features of a few micrometers was computationally investigated. The device considered is a corona–dielectric barrier similar to industrial web-treatment devices [32], and is shown schematically in figure 1 as implemented in the model. The geometry is symmetric across the centerline. The upper metal electrode is housed in a dielectric with an exposed tip and is typically powered at a few to 10 kHz. The gap between the tip of the upper electrode and the lower grounded metal electrode is 2 mm. The rough PP surface is

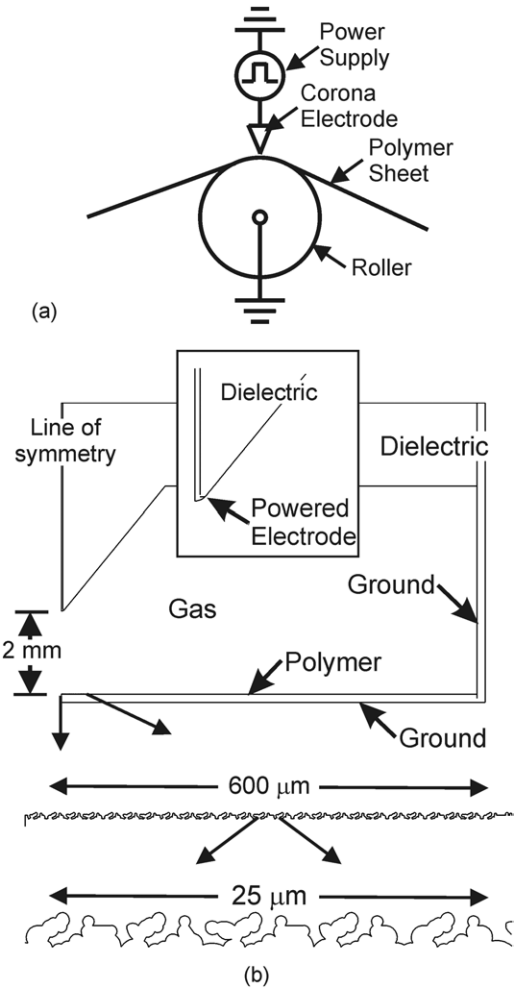

Figure 1. Schematic of the corona treatment device. (*a*) Typical web-roller arrangement for polymer treatment. (*b*) Model representation of the discharge device with magnification of the rough polymer surface having micrometer-sized strand-like features.

on the lower grounded electrode and so it effectively operates as a dielectric-barrier discharge. Roughness on the polymer surface is resolved having strand-like features of a few micrometers to resemble textiles or scaffold-like surfaces for cell adhesion. Note that the fine surface structure is included only within 600 μm of the centerline to reduce the computational burden. In the following discussion, macroscopic uniformity refers to scale lengths of the discharge, up to a few millimeters. Microscopic uniformity refers to scale lengths of the surface features, many to tens of micrometers. These uniformities are being examined for a stationary surface (that is, a non-moving web) without forced gas flow and so reflect the fundamental processes. As discussed in [20], macroscopic non-uniformities may be averaged out by motion of the web and forced gas flow.

The unstructured mesh is locally refined close to the powered electrode and near the surface features with a resolution of about 1 μm so that reactor- and surface-scale processes can be simultaneously resolved. Regions distant from the discharge zone have node spacings of 100 μm. The total number of nodes is 21 296 with 9643 of these being in the plasma. Results from simulations with a smaller number of surface features and increased resolution did not significantly

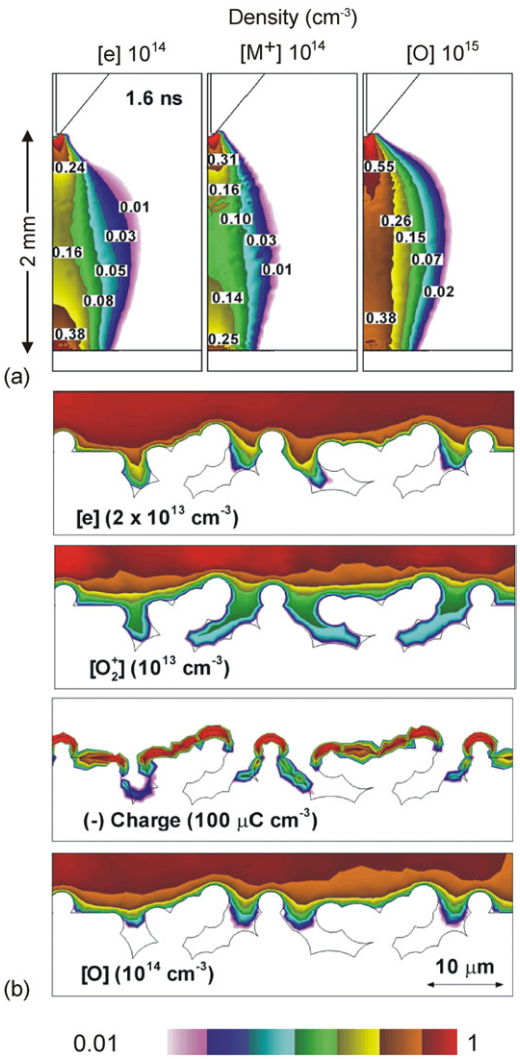

Figure 2. Plasma properties after the first breakdown pulse in a negative humid air discharge. (*a*) Densities of electrons, positive ions and oxygen atoms. (*b*) Densities of electrons, O_2^+, negative surface charge and O atoms in the vicinity of the surface. The contour labels are fractions of the maximum density noted in each figure.

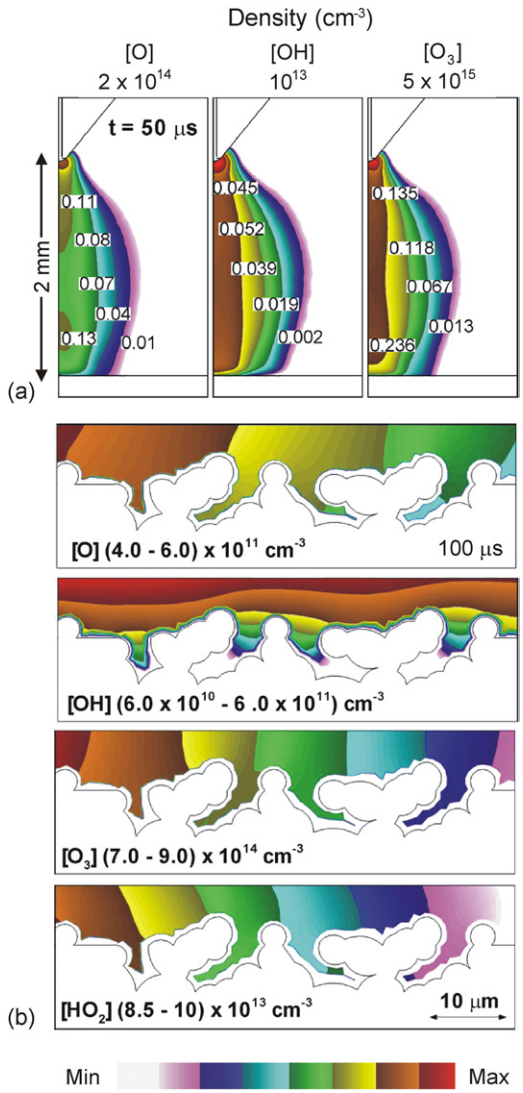

Figure 3. Plasma properties midway during the first interpulse period (duration 100 μs) of the negative discharge. (*a*) Density of O, OH and O_3 in bulk plasma. (*b*) Density of O, OH, O_3 and HO_2 in the vicinity of the surface. The contour labels are fractions of the maximum density noted in each figure.

differ. The base case conditions are atmospheric pressure and $N_2/O_2/H_2O = 79/20/1$ (relative humidity of 30%). The discharge operates at 10 kHz by biasing the powered electrode with unipolar 15 kV pulses of either negative or positive polarity.

The densities of electrons, all positive ions and O atoms at the time the plasma closes the gap after a propagation time of 1.6 ns are shown in figure 2 for a −15 kV pulse. The avalanche, terminated by charging of the PP, produces a plasma density of 10^{13} cm^{-3} in the center of the gap and nearly 10^{14} cm^{-3} at the tip of the electrode. The major radicals for PP processing produced by electron impact dissociation are O and OH with densities of a few times 10^{13} and 10^{12} cm^{-3} in the vicinity of the PP surface.

Densities of electrons, O_2^+, O, OH and surface charges at the end of the discharge pulse near the surface are also shown in figure 2. The electrons and ions are able to penetrate into the surface features only to a limited extent. The size of the features are commensurate with the Debye length ($\lambda_D \approx 1$–$10\,\mu$m). However, at times during and after the pulse, the ion density inside the features is low enough that it is not mandatory that charged particle densities be quasi-neutral. The more mobile electrons in the leading edge of the avalanche negatively charge the surface of the features with local volume densities of up to 100 μC cm^{-3}. This surface charging, which occurs dominantly at sites with large view angles to the plasma, prevents electrons from deeply penetrating into the features. What penetration of electrons there is continues to produce O atoms by electron impact dissociation, though at the end of the discharge pulse, radicals are largely absent from deep inside the features. Positive ions are accelerated into the features by the negative surface charge and fill the features with densities of 10^{11} cm^{-3}.

The densities of O, O_3 and OH at 50 μs, halfway through the IP, are shown in figure 3(*a*). At this time, the peak density of O atoms in the discharge region has been reduced by more

than an order of magnitude largely by the formation of O_3, producing an ozone density of nearly 10^{15} cm^{-3}. Since the main pathway for gas phase production of OH is electron impact of H_2O, the density of OH steadily decreases during the IP in the bulk.

The densities of O, OH, O_3 and HO_2 near the surface features near the end of the IP of 100 μs are shown in figure 3(*b*). At this late time, diffusion has enabled the densities of species that slowly react with the surface to be essentially uniform over the scale of the roughness. Neutral radicals continue to penetrate into surface features by diffusion. O atoms, further depleted by the formation of O_3 and reactions with the surface, have densities of 5×10^{11} cm^{-3} inside the features. O_3 and HO_2, species which tend to accumulate due to their low reactivity, have densities of 8×10^{14} and 9×10^{13} cm^{-3} inside the features. Earlier in the IP, the surface is a net source of OH as a result of H abstraction by O atoms. By the end of the IP, these sources decrease with the depletion of the O atoms. As a result, the surface becomes a net sink for OH given its own reactivity with the surface, and the density of OH inside features decreases.

The densities of electrons, positive ions and O atoms during breakdown for a positive voltage pulse are shown in figure 4(*a*). As is characteristic of positive corona streamers compared with negative streamers, the plasma column is more confined because the positive corona is more critically dependent on space charge and photoionization for propagation. However, the charged particle densities in the bulk plasma are commensurate between the positive and the negative discharges. With electrons drifting upwards, when the avalanche strikes the surface charging is positive and the discharge spreads out forming a sheath like, cathode fall region at the surface. The source of electrons in this region is dominantly by secondary emission by ions from the surface. The bulk of the ions are driven into the features by electric field drift producing densities of 10^{11}–10^{12} cm^{-3} and surface charge of up to a positive 1 μC cm^{-3}. Since few electrons enter into the features ($<10^{10}$ cm^{-3}) and secondary electrons are not numerous, there is negligible O atom production and density inside the features during the pulse. Recombination of O^+ ions on the surface is a larger source.

The densities of O, OH and O_3 at the end of the IP at 100 μs are shown in figure 5(*a*). Similar to the negative discharge, the density of O atoms decreases by a factor of 10–100 during the interpulse period largely by the formation of O_3. The density of OH decreases due to gas phase and surface reactions, and diffusion to about 10^{12} cm^{-3} while the density of O_3 increases to 10^{15} cm^{-3}. The densities of O, OH, O_3 and HO_2 near the surface features late during the IP at 90 μs are shown in figure 5(*b*). The trends are similar to the negative pulse; however, the densities of O and OH are higher by an order of magnitude.

The time-averaged fluxes of O, OH, H and O_3 during one discharge period as a function of position along the PP surface for positive and negative discharges are shown in figure 6. Despite the higher O atom densities created near the surface during the pulse in the positive discharge, the average flux of O atoms are similar for both polarities. Since penetration of

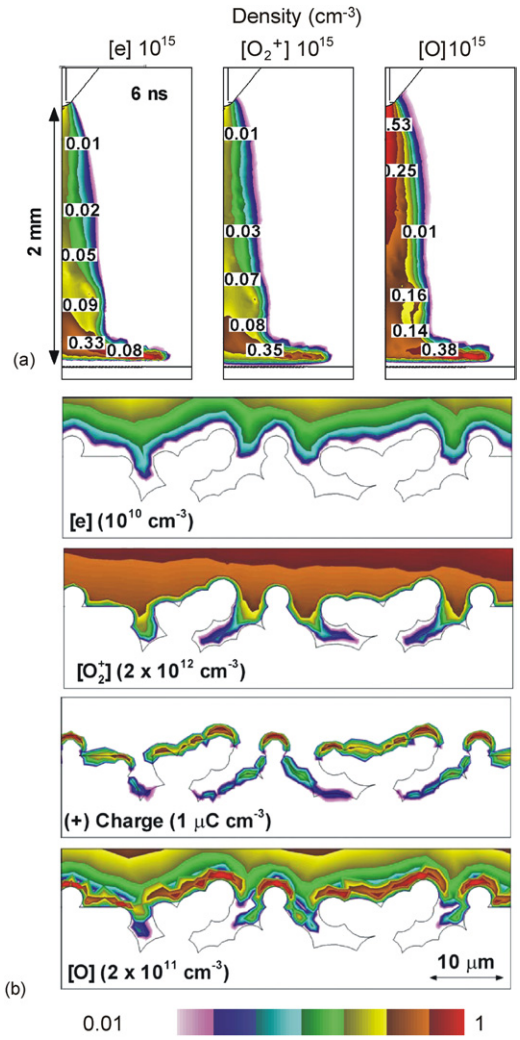

Figure 4. Plasma properties after the first breakdown pulse in a positive humid air discharge. (*a*) Densities of electrons, O_2^+ and oxygen atoms. (*b*) Densities of electrons, O_2^+, positive surface charge and O atoms in the vicinity of the surface. The contour labels are fractions of the maximum density noted in each figure.

plasma into the features during the positive discharge pulse is low, the more numerous O atoms are consumed in the gas phase as they diffuse into the features, and so the fluxes end up being commensurate to the negative discharge. However, the microscopic gradients in O atom fluxes are larger in the positive discharge. The fluxes of OH are higher in the positive discharge by a factor of 2–10 owing to their lower gas phase reactivity. However, OH reacts rapidly with the surface, and this consumption creates significant microscopic variation in OH fluxes inside features. Sites having larger view angles to the plasma tend to receive larger fluxes.

The fluxes of O_3 are higher in the positive discharge due to the larger density of O atoms generated during the pulse. The spatial trends in O_3 fluxes track those of O atoms. In general, the macroscopic variation in fluxes arises from the original spatial distribution of radicals in the discharge at the termination of the pulse, and subsequent gas kinetic reactions and transport. In spite of its wider bulk plasma channel, macroscopic gradients are larger with the negative discharge. The spreading of the plasma along the surface in the narrower

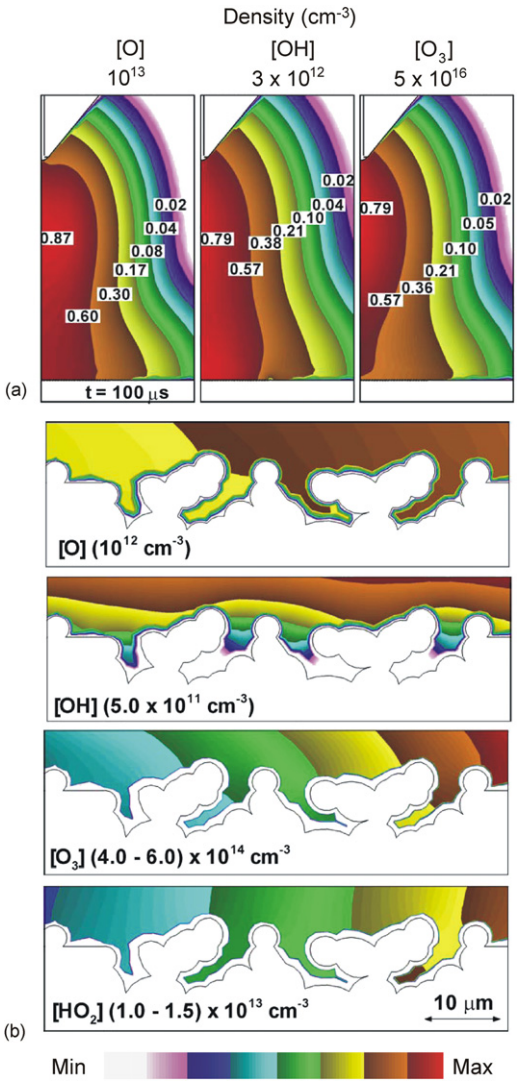

Figure 5. Plasma properties at the end of the first interpulse period (duration 100 μs) of the positive discharge. (*a*) Densities of O, OH and O_3 in bulk plasma. (*b*) Densities of O, OH, O_3 and HO_2 in the vicinity of the surface. The contour labels are fractions of the maximum density noted in each figure.

positive discharge provides for more uniform fluxes on the macroscopic scale.

The densities surface groups on the PP in the negative discharge during a single IP period [alkyl, (R•)] and after several IPs [alkoxy (R–O•) and peroxy (R–OO•)] are shown in figure 7. Alkyl radicals are rapidly generated during and immediately after a discharge pulse by abstraction of H atoms from the PP backbone by O and OH created within a few mean-free paths of the surface. The alkyl coverage reaches a maximum fractional value of 2×10^{-5} (2×10^{10} cm^{-2}) a few microseconds into the IP. For the remainder of the IP, alkyl sites are consumed by O, O_3 and O_2 from the gas phase producing alkoxy (R–O•) and peroxy (R–OO•) groups. This reduces the density of alkyl sites to $<10^9$ cm^{-2}. This cycle of production and consumption of alkyl sites is repeated with every discharge pulse and IP. The local maxima in alkyl coverage are for those surface sites that have large view angles of the plasma, and so receive larger fluxes of O and OH.

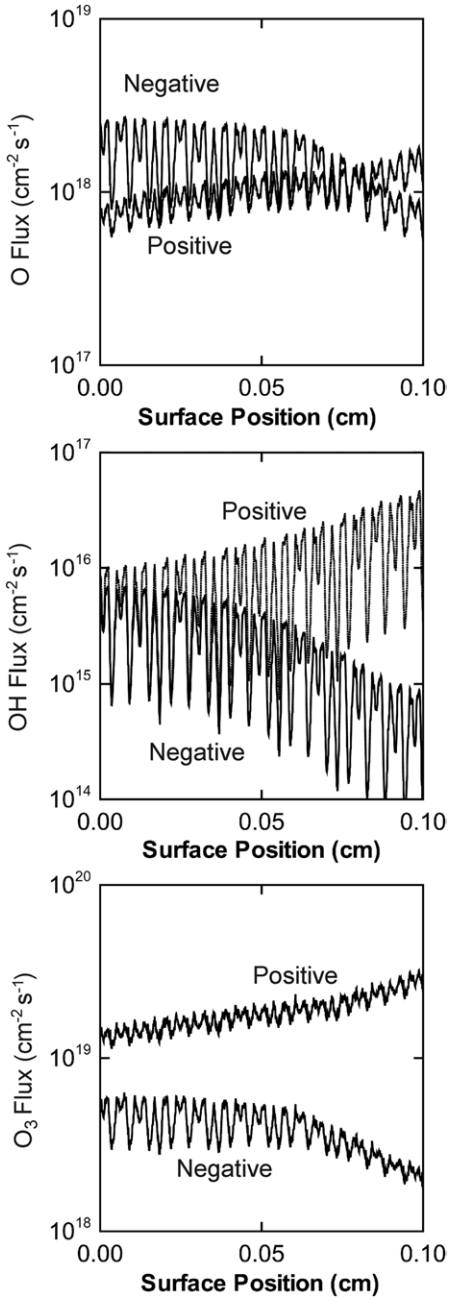

Figure 6. Effect of voltage polarity on time-averaged fluxes with position along the rough PP surface for positive and negative discharge polarities. (*a*) O, (*b*) OH and (*c*) O_3.

Unlike the cyclic behavior of alkyl (R•) sites, the densities of alkoxy (R–O•) and peroxy (R–OO•) groups increase with treatment time as shown in figure 7. As alkoxy and particularly peroxy groups only slowly react with gas phase species, their densities increase from pulse to pulse as they are created from alkyl sites. The macroscopic uniformities of coverage of alkoxy and peroxy groups depend on the spatial gradients in the O and O_3 fluxes, and so their coverages are highest on axis. The gradient is more severe for alkoxy sites since both the fluxes of O and O_3 are largest on axis, both creating the precursor alkyl sites and passivating those sites. The peroxy sites are formed from alkyl sites by passivation with O_2 which does not have a macroscopic spatial gradient.

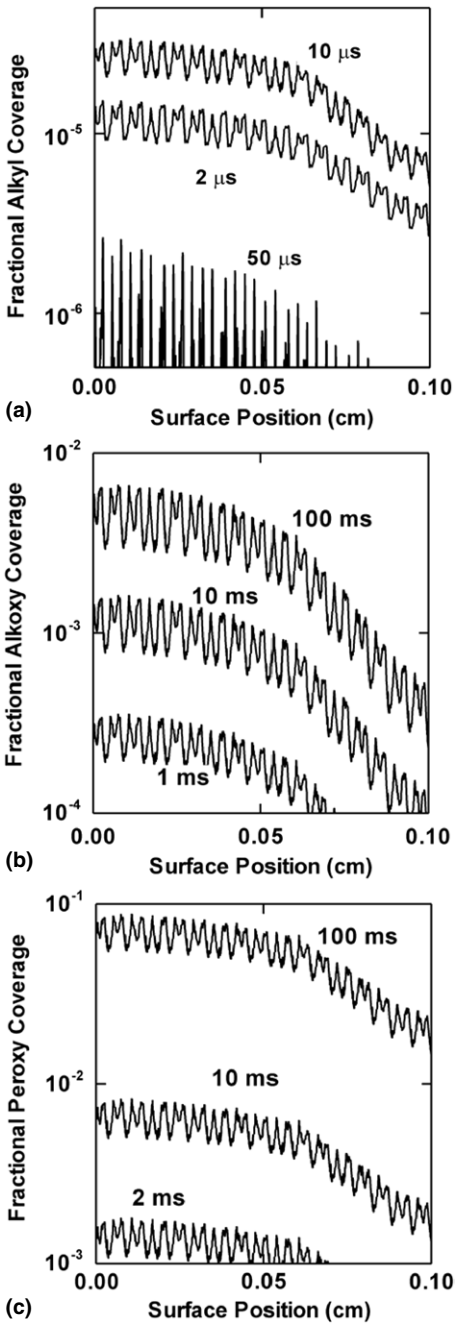

Figure 7. Coverage of functional groups with position along the rough surface in repetitively pulsed negative discharges at different times. (*a*) alkyl radicals (R•), (*b*) alkoxy (R–O•) and (*c*) peroxy (R–OO•).

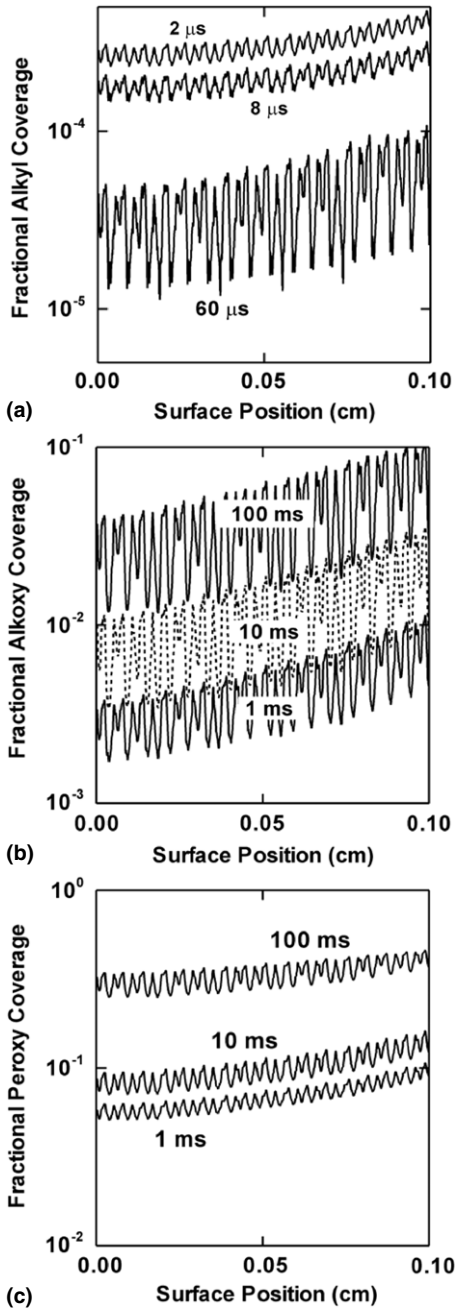

Figure 8. Coverage of functional groups with position along the rough surface in repetitively pulsed positive discharges at different times. (*a*) alkyl radicals (R•), (*b*) alkoxy (R–O•) and (*c*) peroxy (R–OO•).

The analogous time evolutions of alkyl (R•), alkoxy (R–O•) and peroxy (R–OO•) coverages in the positive discharge are shown in figure 8. As with the negative discharge, the alkyl sites are regenerated during and immediately after each pulse, but to densities in excess of 2×10^{11} cm^{-2} due to the larger fluxes of OH. These sites are consumed by passivation dominantly by O_3 and O_2 in the interpulse period. In contrast to the negative discharge, there is greater uniformity on the scale of a few millimeters. This results from the spreading of the positive discharge on the PP, which reduces spatial gradients in the fluxes of O and O_3. However, slower radical penetration into features results in increased microscopic non-uniformity of alkoxy sites.

The coverage of alcohol (R–OH) and carbonyl (R–C=O) groups after 1 s of treatment is shown in figure 9 for positive and negative discharges. There are qualitative differences in both small-scale and large-scale coverages. Although the negative corona has higher coverages of carbonyl groups on axis, the more local production of O and OH in the positive corona discharges at larger radii increases the coverage of all groups at larger radii. Microscopic variations in both carbonyl and alcohol groups are larger in the positive discharge, similar to that of the alkoxy coverage. The larger fluxes of more reactive

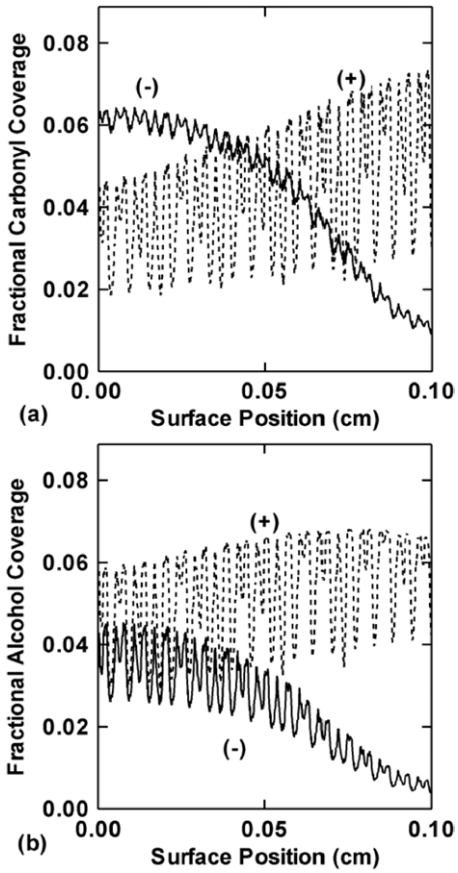

Figure 9. Coverage of selected groups along the rough surface after 1 s treatment in repetitively pulsed negative and positive discharges (*a*) carbonyl (R–C=O) and (b) alcohol (R–OH).

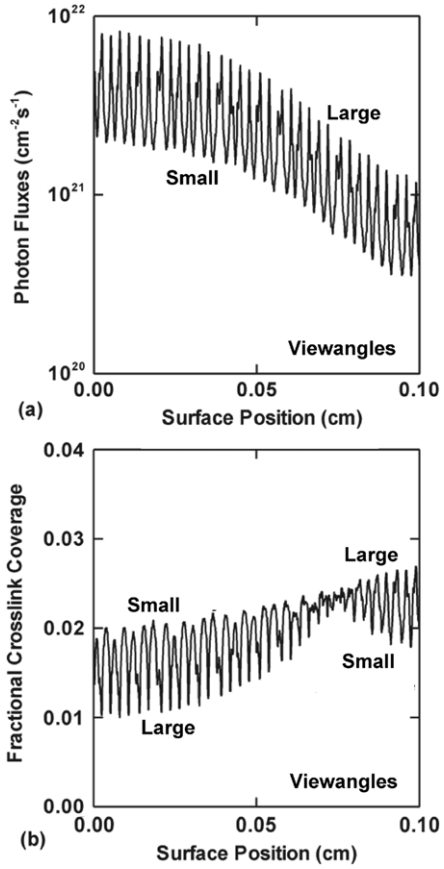

Figure 10. Photon properties and photon initiated products for a negative discharge. (*a*) Photon fluxes at the end of the discharge pulse and (*b*) density of crosslinked sites after 1 s of treatment. The sharp microscopic variations arise due to line of sight photon transport being shadowed by surface features.

OH provides for higher and more uniform peak coverage but differentiates more between sites having larger and smaller view angles to the plasma. As such, the choice of polarity of the discharge does give some degree of control of composition and uniformity. Positive corona discharges tend to have more macroscopic uniformity due to the spreading of the discharge across the surface. At the same time, positive discharges have less microscale uniformity due to the limited ability for electrons to penetrate deeper into the microstructure where they may produce radicals.

Through parametrization of the model and sensitivity studies of reaction probabilities, it was found that the most likely role of low energy ions—abstracting H atoms from PP to create alkyl radical sites—was not significant in atmospheric pressure corona discharges. The reaction probability for an ion M^+ reacting with a PP site to abstract an H atom,

$$M^+ + RH \rightarrow R^\bullet + M\text{–}H, \tag{32}$$

was varied between 10^{-3} and 1.0. The resulting change in surface functionalization over a treatment time of 1 s was negligible. This was to be expected since the ions have a much shorter lifetime compared with neutral radicals and their densities do not accumulate pulse to pulse. As a result, their time-averaged fluxes to the surface are generally orders of magnitude smaller than O, OH and O_3. Although low energy ions might also produce chain scission and crosslinking, the low fluxes of ions (and lack of accumulation on a pulse-to-pulse basis) reduce the importance of these processes.

Crosslinking is a terminal process for consumption of surface radical sites by creating non-reactive sites. Crosslinking can be a significant process when the flux of reactive gas species is low, such as in rare gas discharges. In discharges where the flux of passivating species is large, the likelihood for radical sites to react with and be passivated by gas phase species prior to crosslinking is large. UV photons from the plasma contribute to crosslinking by adding another pathway for chain scission reactions.

For example, the UV photon flux along the surface at the end of breakdown for a −15 kV discharge pulse is shown in figure 10(*a*). These fluxes generally track the spatial gradients in plasma density. The line of sight transport of photons results in shadowed surface features receiving a lower photon flux than sites that are directly exposed to the discharge. The density of crosslinked sites resulting from the UV illumination after 1 s of processing is shown in figure 10(*b*). Crosslinking competes with functionalizing and passivating gas phase reactions. At those sites where fluxes of reactive gas phase species is large, surface radicals are more likely to be passivated than crosslinked. For the negative discharge, these fluxes are highest on axis and so the density of crosslinked sites is lower on axis. For the same reasons, the densities of crosslinked sites

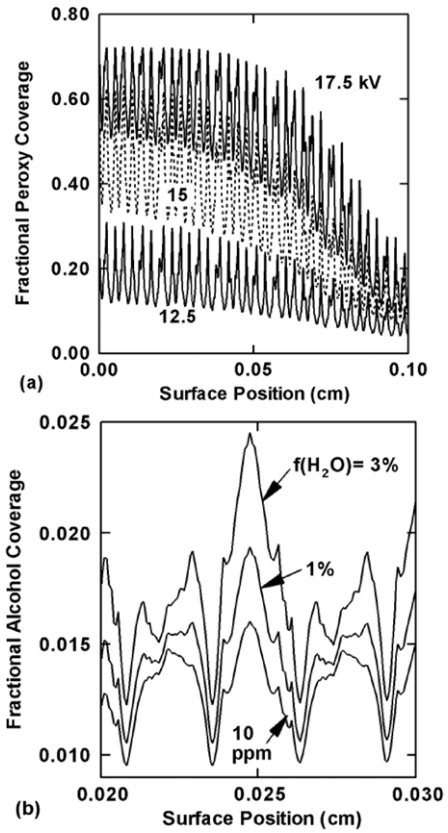

Figure 11. Surface properties after 1 s treatment in repetitively pulsed discharges. (*a*) Surface coverage of peroxy (R–OO•) for −12.5, −15 and −17.5 kV. (*b*) Surface coverage of alcohol (R–OH) groups while varying the relative humidity.

are larger inside features on axis than outside the features. This results from the fluxes of passivating species being lower inside the features but there being sufficient penetration of the plasma into features that produces photons that photon produced chain scission reactions occur. Off axis, the penetration of plasma into features is less and the shadowing of photon fluxes from the high plasma density regions is more severe. In those locations, there is more photon-induced crosslinking at the top of features than inside features.

The consequences of the magnitude of the negative applied voltage on the coverage of peroxy groups (R–OO•) after 1 s of treatment are shown in figure 11(*a*) With an increase in applied voltage, the densities of radicals generated in the discharge increase and so surface coverages increase. The macroscopic uniformity decreases with increasing voltage due to a narrowing of the discharge (more rapid gap closure) producing larger gradients in radical production. These higher fluxes on axis begin to saturate the surface sites at about 0.7 coverage. Microscopic variations in coverage do not change significantly as the local spatial dynamics of reactive species fluxes are not sensitive functions voltages.

Relative humidity or the fraction of H_2O, $[f(H_2O)]$ in air ultimately determines the densities of OH generated in the discharge. Larger $f(H_2O)$ generally produce larger fluxes of OH. These radicals contribute both to more rapid H abstraction and to the slower OH addition to alkyl (R•) sites producing alcohol (R–OH) groups. The effect of $f(H_2O)$ on the coverage of alcohol groups is shown in figure 11(b). At low $f(H_2O)$, tens of ppm, the large fluxes of O atoms that abstract H atoms locally produce OH densities that are comparable to the plasma produced flux of OH in discharges having high $f(H_2O)$ of a few per cent. As a result, increasing $f(H_2O)$ has a limited effect on functionalization and production of alcohol groups on the macroscopic scale. Since plasma produced OH fluxes come from outside of the features and OH radicals have larger reaction probabilities with the surface, there is little penetration of plasma produced OH into features. The OH fluxes inside features dominantly result from H abstraction by O atoms. As a result, the alcohol coverage outside features is more sensitive to $f(H_2O)$ than inside features.

4. Concluding remarks

The functionalization of rough PP surfaces with features of a few micrometers using repetitively pulsed atmospheric pressure discharges in humid air was computationally investigated. Electrons and ions produced during the pulse penetrate into the rough surface features to a limited extent. The penetration of charged species depends on the discharge polarity. In negative discharges, there is limited penetration of electrons into surface features which locally produce reactive species by electron impact. In positive discharges a sheath-like region near the surface prevents electrons from penetrating into the surface features and so there is less local production of radicals. Longer lived radicals are able to penetrate into all surface features over timescales of hundreds of microseconds. The more reactive radicals such as OH are depleted near exposed surface features which reduces fluxes penetrating inside the features. In atmospheric pressure discharges, the contributions of ions to surface chemistry are limited. Although the contribution of UV photons is small, some crosslinking does occur at locations where reactive fluxes of passivating radicals are low.

The dynamics of the discharge and radical generation have significant effects on the degree and uniformity of functionalization. The macroscopic distribution of reactive species in the positive discharge is more uniform due to spreading of the discharge along the surface, and this leads to higher macroscopic uniformity of treatment. However poor plasma penetration into features produces more microscopic non-uniformities than in the negative discharge. Increasing humidity had a limited effect on alcohol coverage due to the formation of OH at the surface by H abstraction by O atoms.

Acknowledgments

This work was supported by the National Science Foundation (CTS-0520368). The authors thank Dr Mark Strobel for his advice and guidance.

References

[1] Liston E M, Martinu L and Wertheimer M R 1993 *J. Adhes. Sci. Technol.* **7** 1091
[2] Sun C, Zhang D and Wadsworth L C 1999 *Adv. Polym. Technol.* **18** 171

[3] Strobel M, Lyons C S and Mittal K L (ed) 1994 *Plasma Surface Modification of Polymers* (Zeist, The Netherlands: VSP Press)
[4] Lynch J B, Spence P D, Baker D E and Postlethwaite T A 1999 *J. Appl. Polym. Sci.* **71** 319
[5] O'Hare L-A, Leadley S and Parbhoo B 2002 *Surf. Interface Anal.* **33** 335
[6] Borcia G, Anderson C A and Brown N M D 2004 *Appl. Surf. Sci.* **221** 203
[7] Carneiro N, Souto A P, Silva E, Marimba A, Tena B, Ferreira H and Magalhaes V 2001 *Coloration Technol.* **117** 298
[8] Hoecker H 2002 *Pure Appl. Chem.* **74** 423
[9] Kan C W 2007 *J. Adhes. Sci. Technol.* **21** 911
[10] Poll H U, Schladitz U and Schreiter S 2001 *Surf. Coat. Technol.* **142–144** 489
[11] De Geyter N, Morent R and Leys C 2006 *Plasma Sources Sci. Technol.* **15** 78
[12] Vohrer U, Muller M and Oehr C 1998 *Surf. Coat. Technol.* **98** 1128
[13] Tsai P P, Roth J R and Chen W W 2005 *Textile Res. J.* **75** 819
[14] Castner D G and Ratner B D 2002 *Surf. Sci.* **500** 28
[15] Pu F R, Williams R L, Markkula T K and Hunt J A 2002 *Biomaterials* **23** 2411
[16] Jones I, Currie L and Martin R 2002 *Br. J. Plast. Surg.* **55** 185
[17] Chim H, Ong J L, Schantz J-T, Hutmacher D W and Agrawal C M 2002 *J. Biomed. Mater. Res.* A **65A** 327
[18] Lee J H, Kim H W, Pak P K and Lee H B 1994 *J. Polym. Sci.* A **32** 1569
[19] Bhoj A N and Kushner M J 2008 *Plasma Sources Sci. Technol.* **17** 035025
[20] Bhoj A N and Kushner M J 2007 *J. Phys. D: Appl. Phys.* **40** 6953
[21] Dorai R and Kushner M J 2003 *J. Phys. D: Appl. Phys.* **36** 666
[22] Tochikubo F, Chiba T and Watanabe T 1999 *Japan. J. Appl. Phys.* **38** 5244
[23] Wertheimer M R, Fozza A C and Hollander A 1999 *Nucl. Instrum. Methods Phys. Res.* B **151** 65
[24] Wilken R, Hollander A and Behnisch J 1999 *Surf. Coat. Technol.* **116–119** 991
[25] Truica-Marasescu F, Jedrzejowski P and Wertheimer M R 2004 *Plasma Proc. Polym.* **1** 153
[26] Skurat V E and Dorofeev Y I 1994 *Angew. Makromol. Chem.* **216** 205
[27] Kuvaldina E V, Rybkin V V, Titov V A, Shikova T G and Shutov D A 2004 *High Energy Chem.* **38** 411
[28] Poncin-Epaillard F, Vallon S and Drevillon B 1997 *Macromol. Chem. Phys.* **198** 2439
[29] Poncin-Epaillard F, Brosse J C and Falher T 1997 *Macromolecules* **30** 4415
[30] Hong J, Truica-Marasescu F, Martinu L and Wertheimer M R 2002 *Plasmas Polym.* **7** 245
[31] Hansen R H and Schonhorn H 1966 *J. Polym. Sci. Lett.* B **4** 203
[32] Strobel M, Jones V, Lyons C S, Ulsh M, Kushner M J, Dorai R and Branch M C 2003 *Plasmas Polym.* **8** 61